Turbulent Droplet Breakage Probability: Analysis of Fitting Parameters for Two Commonly Used Models

Krishnamurthy Ravichandar, Michael G. Olsen

Department of Mechanical Engineering, Iowa State University, Ames, IA 50011

R. Dennis Vigil*

Department of Chemical & Biological Engineering, Iowa State University, Ames, IA 50011

Abstract

Although several mathematical models have been developed to describe droplet breakage in agitated liquid emulsions, the utility of these models is limited by the fact that they incorporate multiple fitting parameters that must be determined empirically for specified fluid pairs and flow conditions. In this work, analytical expressions that can be evaluated without need to perform droplet breakage experiments have been developed for parameters associated with droplet breakage probability in two commonly used breakage models. Data used for validation of the proposed equations for the breakage probability parameters were obtained from previously published reports of droplet breakage in heterogeneous flow devices and from experiments performed in a von Kármán box designed to produce homogeneous turbulence. Comparison of the droplet breakage probability predictions using the derived expressions for the breakage parameters show generally good agreement with experimental data.

Keywords: Drop Breakup, Emulsions, Droplets, von Kármán Box

1. Introduction

The breakage of dispersed liquid droplets immersed in a second immiscible liquid phase is an important phenomenon in the production of petrochemicals, polymers [1], metals, foods [2], and pharmaceuticals [3, 4], and it is also vital for environmental management, such as clean up of oil spills [5, 6] and leaks from underground storage tanks. Droplet breakage has a substantial impact on interphase mass transfer in chemical processing equipment, such as in liquid extractors and liquid-liquid reactors [7], because it impacts the evolution of interfacial area between dispersed and continuous phases. Consequently, accurate and validated models for droplet breakage are needed to optimize equipment design and operation.

*Corresponding author

URL: vigil@iastate.edu (R. Dennis Vigil)

A comprehensive predictive breakage model that incorporates accurate descriptions of the many hydrodynamic processes that can contribute to drop breakage under various flow conditions does not currently exist, and such a model will likely not be realized in the near future due to incomplete understanding of multiphase flow physics. However, several mathematical models have been developed to describe droplet breakage in using various assumptions [8–12], and such models can provide useful information provided that they are employed in situations for which the model assumptions are applicable. However, even for models that incorporate many simplifying assumptions, empirically-determined fitting parameters are usually required to compensate for the lack of closure relations for the underlying turbulent flow phenomena. For such models, the existence of universal parameter values is unlikely [13], and therefore it is necessary to carry out a large number of experiments to generate sufficient information to estimate the values of these parameters for a given set of fluid pairs and flow conditions.

Acquisition of experimental data for fitting of model parameters is difficult due to the nature and quantity of the information that is required, including breakage probability, breakage time, and child droplet size distribution as functions of parent drop size, turbulence dissipation rate, and other flow descriptors. Such information is usually obtained using optical methods to observe breakage of droplets introduced into a turbulent media, one at a time. A wide variety of experimental flow geometries have been used to perform such experiments, which further complicates the task of parameter fitting [3, 14–22]. Consequently, comparison of results from these various studies is difficult, since differences in flow geometry give rise to different breakage mechanism contributions (e.g. turbulent fluctuations, droplet-wall, or droplet-droplet collisions) to the overall observed statistics [23]. Moreover, breakage models are usually expressed in terms of quantities such as turbulence dissipation rate, ε, and appropriate values for this quantity can be difficult to determine due to the heterogeneity of typical equipment used to collect drop breakage data, such as stirred tanks [24–26].

The purpose of this work is to show how some fitting parameters associated with droplet breakage probability for two well-known and widely used breakage models can be estimated without the need to perform experiments. The analysis described in the next section applies only to the models considered, both of which incorporate numerous assumptions (including neglect of breakage mechanisms other than those due to turbulent fluctuations) and therefore no universality is claimed. The approach used here is to derive analytical expressions for parameters associated with droplet breakage probability by applying dimensional analysis and by using a hypothesis regarding breakage probability that is based upon competition between disruptive and restorative stresses on droplets. The validity of the resulting equations for calculating breakage parameters *a priori* is then evaluated by comparing the predictions with those obtained by fitting the breakage parameters to experimental data. The experimental data used for validation was obtained from two sources including (1) previously published reports of droplet breakage in stirred tanks and in pipe flow and (2) experiments peformed in a von Kármán box designed to produce homogeneous turbulence.

2. Breakage Probability Parameters

2.1. Breakage Models

Several breakup models have been developed and applied with some success to simulate droplet breakage in process equipment. These models are usually based upon consideration of various disruptive and cohesive stresses that occur upon the collision of droplets with turbulent eddies. The relative magnitudes of the various competing stresses depend upon numerous factors such as parent droplet size, local turbulence dissipation rate, density and viscosity of the liquid phases, and liquid-liquid interfacial tension.

Here we restrict ourselves to cases in which droplet breakage is primarily determined by competition between the disruptive turbulent stress exerted on a droplet and the cohesive interfacial and/or internal viscous stresses. This regime is relevant to many important practical applications, such as the processing of petroleum-water mixtures and vegetable oil-water emulsions. The classic Coulaloglou-Tavlarides breakage model [27] describes the situation in which internal viscous stresses may be neglected so that droplet breakage is determined by competition between turbulent and interfacial stresses, and it can be expressed as follows:

$$r_b(d) = a(d)c(d) \tag{1}$$

$$a(d) = C_1 \varepsilon^{1/3} d^{-2/3} \exp\left[-\frac{C_2 \sigma}{\rho_d \varepsilon^{2/3} d^{5/3}}\right] \tag{2}$$

Here, $r_b(d)$ and $c(d)$ represent the overall breakage rate (breakage events/volume/time) and the concentration of droplets having characteristic diameter d, respectively. The term $a(d)$ is a breakage rate coefficient having units of inverse time. In Eq.(2), C_1 and C_2 are system-specific constants, ρ_d represents the mass density of the droplet phase, and σ is the interfacial tension between droplets and the continuous phase. The derivation of Eq.(2) will not be repeated here, but it is worth noting that the exponential term, which describes the probability of drop breakage, arises as a consequence of two major assumptions, namely that droplets have the same energy distribution as turbulent eddies, and that only eddies smaller than droplets are effective for breakup. The term $C_1 \varepsilon^{1/3} d^{-2/3}$ can be equated with the inverse breakage time associated with a droplet undergoing collision with a turbulent eddy. Equation (2) considers disruptive turbulent deformation (τ_d) and capillary interfacial (τ_σ) stresses [28, 29], defined as

$$\tau_d = 2\rho_c (\varepsilon d)^{2/3} \tag{3}$$

$$\tau_\sigma = \frac{\sigma}{d} \tag{4}$$

The Coulaloglou-Tavlarides model has been extended by several investigators, including Chen *et al.* [30] who generalized it by considering droplet internal viscous stress, τ_μ, [31] given by

$$\tau_\mu = \frac{\mu_d}{d} \left(\varepsilon d\right)^{1/3} \sqrt{\frac{2\rho_c}{\rho_d}}, \tag{5}$$

where ρ_c is the density of the continuous phase and μ_d is the dynamic viscosity of the dispersed droplets. Inclusion of internal viscous stress in the analysis for droplet breakage leads to the following expression:

$$a(d) = \frac{1}{t_b} \exp\Big[-\frac{C_2\sigma}{\rho_d \varepsilon^{2/3} d^{5/3}}\Big] \exp\Big[-\frac{C_3\mu_d}{\rho_d \varepsilon^{1/3} d^{4/3}}\Big] \tag{6}$$

Here, t_b is the droplet breakage time, which Chen and co-workers assumed to be constant. A comparison of Eqs.(2) and (6) shows that including consideration of internal viscous stress in the analysis leads to diminished droplet breakage probability, particularly for highly viscous droplets.

2.2. Dimensionless Breakage Equations

Since the Coulaloglou-Tavlarides breakage model (2) only includes deformation and interfacial stresses, it can be cast in dimensionless form by making use of the Weber number, defined as:

$$\mathrm{We} = \frac{\tau_d}{\tau_\sigma} = \frac{2\rho_c \varepsilon^{2/3} d^{5/3}}{\sigma} \tag{7}$$

Here we draw attention to the portion of Eq.(2) representing breakage probability, P_b, given by

$$P_b = \exp\Big[-\frac{C_2\sigma}{\rho_d \varepsilon^{2/3} d^{5/3}}\Big] = \exp\Big[-\frac{C_2}{\mathrm{We}}\frac{2\rho_c}{\rho_d}\Big] \tag{8}$$

The Chen model (6) includes internal viscous stress in addition to turbulent deformation and interfacial stresses, and therefore it can be expressed in dimensionless form by using both the Weber number and the capillary number, Ca, defined here as [4]:

$$\mathrm{Ca} = \frac{\mu_d}{\sigma}(\varepsilon d)^{1/3}\sqrt{\frac{2\rho_c}{\rho_d}}. \tag{9}$$

Rearrangement of the arguments of the breakage probability terms in Eq.(6) leads to

$$P_b = \exp\Big[-\frac{C_2}{\mathrm{We}}\frac{2\rho_c}{\rho_d}\Big] \exp\Big[-\frac{C_3\mathrm{Ca}}{\mathrm{We}}\sqrt{\frac{2\rho_c}{\rho_d}}\Big] \tag{10}$$

Note that Eq.(10) recovers the Coulaloglou-Tavlarides expression for breakage probability when $\mathrm{Ca}/\mathrm{We} << 1$.

2.3. Evaluation of Breakage Model Constants

An analytical expression for the breakage model constant C_2 can be obtained using Eq.(8) if the breakage probability is known for a specific value of We. Since the Coulaloglou-Tavlarides model was derived by considering only the deformation and interfacial stresses, it is reasonable to hypothesize that the condition for a droplet to have an equal probability of breaking or not is given by $\tau_d = \tau_\sigma$ so that

$$\frac{\sigma_d}{d_{50}} = 2\rho_c(\varepsilon d_{50})^{2/3} \tag{11}$$

and where d_{50} represents the diameter of a droplet with breakage probability $P_b = 0.5$. The above relation can be expressed in terms of the Weber number associated with P = 0.5, so that from Eq.(7) we obtain:

$$\mathrm{We}_{50} = 1 \tag{12}$$

Hence, substituting Eq.(12) into Eq.(8) and setting $P_b = 0.5$ leads to the following expression:

$$C_2 = \frac{\rho_d}{2\rho_c} \ln(2). \tag{13}$$

Thus, it can be anticipated that C_2 depends only on the density ratio of the dispersed and continuous phase liquids. In many liquid-liquid operations of practical importance, namely those involving oil and aqueous phases, the liquid density ratio is of order one and therefore $C_2 \approx \ln(2)/2$. The validity of Eq.(13) can be evaluated by comparing droplet breakage probability predictions using this equation with experimental breakage data, as is discussed in Section 3. It should also be noted that Eq.(13) implies that the drop breakage probability (8) can be expressed as

$$P_b = \left(\frac{1}{2}\right)^{1/\mathrm{We}}. \tag{14}$$

A similar analysis can be performed to estimate the breakage probability constant C_3 in the Chen model, Eq.(6). In analogy with Eq.(11), the condition for $P_b = 0.5$ is for the disruptive and cohesive stresses to be equal such that

$$\tau_d = \tau_\sigma + \tau_\mu \tag{15}$$

Substitution of Eqs.(3) - (5) into Eq.(15) yields an implicit equation for the critical droplet diameter, d_{50}, given by

$$2\rho_c(\varepsilon d_{50})^{2/3} = \frac{\sigma}{d_{50}} + \frac{\mu}{d_{50}}(\varepsilon d_{50})^{1/3}\sqrt{\frac{2\rho_c}{\rho_d}} \tag{16}$$

By using Eqs.(7) and (9), Equation (16) can also be expressed in the dimensionless form

$$\mathrm{We}_{50} = 1 + \mathrm{Ca}_{50}, \tag{17}$$

where once again the subscript emphasizes that the Weber and capillary numbers are evaluated for $P_b = 0.5$. Substitution of the above equation into the expression for breakage probability in the Chen model, Eq. (10), leads to the following prediction for the constant C_3, assuming that C_2 is given by Eq.(13):

$$C_3 = \sqrt{\frac{\rho_d}{2\rho_c}} \ln(2) \tag{18}$$

Equation (18) is nearly identical to Eq.(13) derived earlier for C_2, and a comparison of these two equations shows that they are related as follows:

$$C_3 = C_2\sqrt{\frac{2\rho_c}{\rho_d}}. \tag{19}$$

As was mentioned previously, the density ratio is order unity for many liquid pairs of practical interest, and hence it can be expected that the values for C_2 and C_3 will not differ greatly. Lastly, it should be noted that substitution of Eq.(18) into Eq.(10) gives the following explicit equation for computing breakage probability without need for a fitting constant:

$$P_b = \left(\frac{1}{2}\right)^{(1+\mathrm{Ca})/\mathrm{We}}. \tag{20}$$

As expected, the above expression recovers Eq.(14) for Ca << We.

3. Validation of Breakage Model Parameter Predictions

The development and validation of mathematical models of breakage based upon mechanistic physical understanding of droplet behavior in turbulent flow is challenging not only because of the numerous variables that impact breakage events and the existence of multiple breakage regimes, but also because of the difficulty in acquiring detailed and statistically significant experimental data sets for breakage events carried out under well-controlled conditions. In particular, since droplet breakage strongly depends on the hydrodynamic environment, droplet breakage experiments should ideally be performed in a homogeneous flow field. Nevertheless, most existing experimental studies of turbulent drop breakage were performed using flow devices known to produce heterogeneous mixing environments, such as stirred tanks. Hence, the data used for model validation here was obtained not only from previously published reports of droplet breakage in heterogeneous flows, but also from experiments performed in a von Kármán box designed to produce homogeneous turbulence.

3.1. Validation Using Experimental Data in Heterogeneous Systems

Droplet breakage probability data have previously been reported from experimental studies in channel flows [3, 14, 17], turbulent pipes [15, 16], stirred tanks [21, 22], rotor-stators [20, 32], reciprocating plate columns [33], and impinging jets [34]. Despite the use of such diverse equipment to carry out drop breakage studies, all of these authors made use of the Coulaloglou-Tavlarides models or one of its extensions to compare predictions with experimental data. In each of these previous investigations, droplet breakage probability was determined for various parent droplet diameters (d) from a large ensemble of observed breakage events. The authors of these studies tested a variety of organic droplet phases paired with water as the continuous phase, and the droplet physical properties and estimated turbulence dissipation rates are listed in Table 1. This information can be used in conjuction with water physical property data and parent droplet diameter to compute corresponding ranges of values for We and Ca, also shown in Table 1.

Fitted values for the breakage probability constants C_2 and C_3 can be obtained by regressing the Coulaloglou-Tavlarides (Eq.(2)) and Chen (Eq.(6)) models to droplet breakage probability data. The resulting best-fit breakage probability plots are presented in Figures 1 - 5 as broken lines. The error bars depict 95% confidence envelopes computed by generating drop breakage probability profiles for the minimum and maximum values of C_2 and C_3 that bracket the mean regressed values listed in Table 2. Note that all probability plots use either

Table 1: Organic droplet properties in water and operating parameters reported in droplet breakage studies for toluene and petroleum [17], kerosene and its mixture with surfactant P507 (volume composition indicated) [33], heptane [15, 16], octanol [14], and rapeseed oil [20]. Ranges of parent droplet diameters tested are also listed.

Droplet Phase	ρ **(kg/m^3)**	σ **(mN/m)**	μ **(mPa·s)**	ε **(m^2/s^3)**	d **(mm)**	**We**	**Ca**$\times 10^3$
Toulene	870.0	0.032	0.55	5.19	0.65 - 3.00	1.9 - 37.1	4.5 - 8.2
Petroleum	790.0	0.0385	0.65	5.95	0.55 - 3.10	1.7 - 33.8	4.9 - 8.8
Kerosene	819.2	0.033	2.56	0.091	2.70 - 4.50	0.12 - 2.4	5.5 - 9.9
70% Kerosene	858.3	0.022	3.91	0.091	2.22 - 3.80	0.2 - 3.6	12.2 - 22.2
40% Kerosene	900.5	0.016	9.48	0.091	2.30 - 4.00	0.3 - 5.0	40.0 - 72.2
Heptane	683.7	0.047	0.45	0.416 - 1.31	1.75 - 2.75	0.2 - 10.1	1.2 - 3.3
Octanol	825	0.0082	0.00902	0.0542	0.8 - 2.7	0.34 - 0.93	0.31 - 0.87
Rapeseed Oil	920	0.020	70	535	0.2 - 0.3	0.2 - 4	1.3 - 2.3

We or We/(1+Ca) as the abscissa for ease of comparison with predictions of Eqs. (14) or (20), respectively. The fitted values for C_2 and C_3 are listed in Table 2, and the indicated uncertainties in this table again represent 95% confidence ranges.

Table 2: Comparison of C_2 and C_3 values obtained from predictions of Eqs. (13) and (18) with values obtained by regressing the Coulaloglou-Tavlarides and Chen models to experimental data.

Test fluid	C_2**, Eq.**(13)	C_2**, Coulaloglou Model Regressed**	C_2**, Chen Model Regressed**	C_3**, Eq.**(18)	C_3**, Regressed**
Toulene	0.302	0.416 ± 0.264	0.388 ± 0.245	0.457	0.589 ± 0.371
Petroleum	0.274	0.390 ± 0.158	0.401 ± 0.168	0.436	0.638 ± 0.268
Kerosene	0.284	0.305 ± 0.199	0.273 ± 0.175	0.444	0.427 ± 0.273
70% Kerosene, 30% P507	0.297	0.272 ± 0.112	0.276 ± 0.111	0.454	0.421 ± 0.170
40% Kerosene, 60% P507	0.312	0.287 ± 0.174	0.298 ± 0.168	0.465	0.443 ± 0.251
Heptane ε=0.416 m^2/s^3	0.237	0.250 ± 0.190	0.250 ± 0.190	0.405	0.428 ± 0.325
Heptane ε=0.549 m^2/s^3	0.237	0.261 ± 0.190	0.220 ± 0.151	0.405	0.376 ± 0.259
Heptane ε=1.31 m^2/s^3	0.237	0.145 ± 0.127	0.142 ± 0.142	0.405	0.243 ± 0.243
Octanolε=0.0542 m^2/s^3	0.446	0.305 ± 0.100	0.3003 ± 0.1004	0.693	0.467 ± 0.154
Rapeseed oil ε=535 m^2/s^3	0.320	-	0.411 ± 0.149	0.472	0.606 ± 0.220

Examination of Figs. 1 - 4 shows that the breakage probability curves obtained using the expressions given by Eqs. (14) and (20) are similar to the breakage probability curves obtained by regression to experimental data, except for the largest turbulence dissipation rate case considered for the heptane-water system and Rapeseed oil system. It should be noted that the generally good agreement of predictions based on Eqs. (14) and (20) with regressed breakage probability curves is observed despite the fact that the equipment used to collect the experimental data is known to exhibit heterogeneous turbulence and therefore the reported estimates for the mean turbulence dissipation rates may not be representative of the conditions that are most responsible for droplet breakage events.

Figures 1 - 4 also suggest that there is no significant difference between droplet breakup probability predictions of the Coulaloglou-Tavlarides and Chen models with C_2 and C_3 given by Eqs. (13) and (18), an observation that can be confirmed by comparing the root mean square errors of the model predictions compared to experimental data, as shown in Table 3. Although this result could be attributed to a lack of experimental data sufficient to resolve differences between these models, it can also be seen that the two models produce similar predictions because internal viscous stresses play only a small role in determining breakage

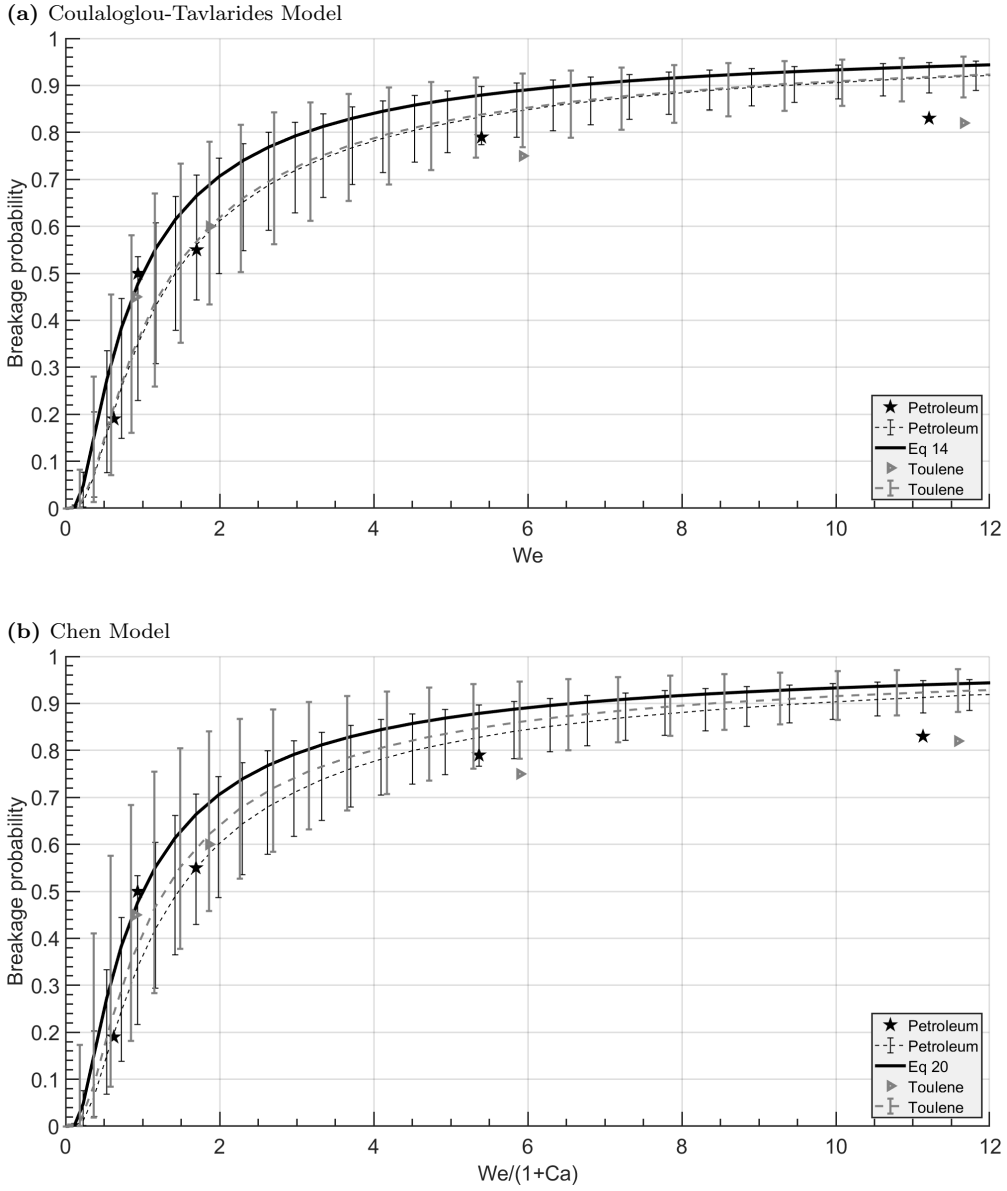

Figure 1: Breakage probability as a function of We and Ca for petroleum-water and toluene-water emulsions. Solid lines represent predictions using Eqs. (14) and (20), dashed lines represent regressions to experimental data, and symbols represent experimental data. Error bars represent 95% confidence intervals for the regressions.

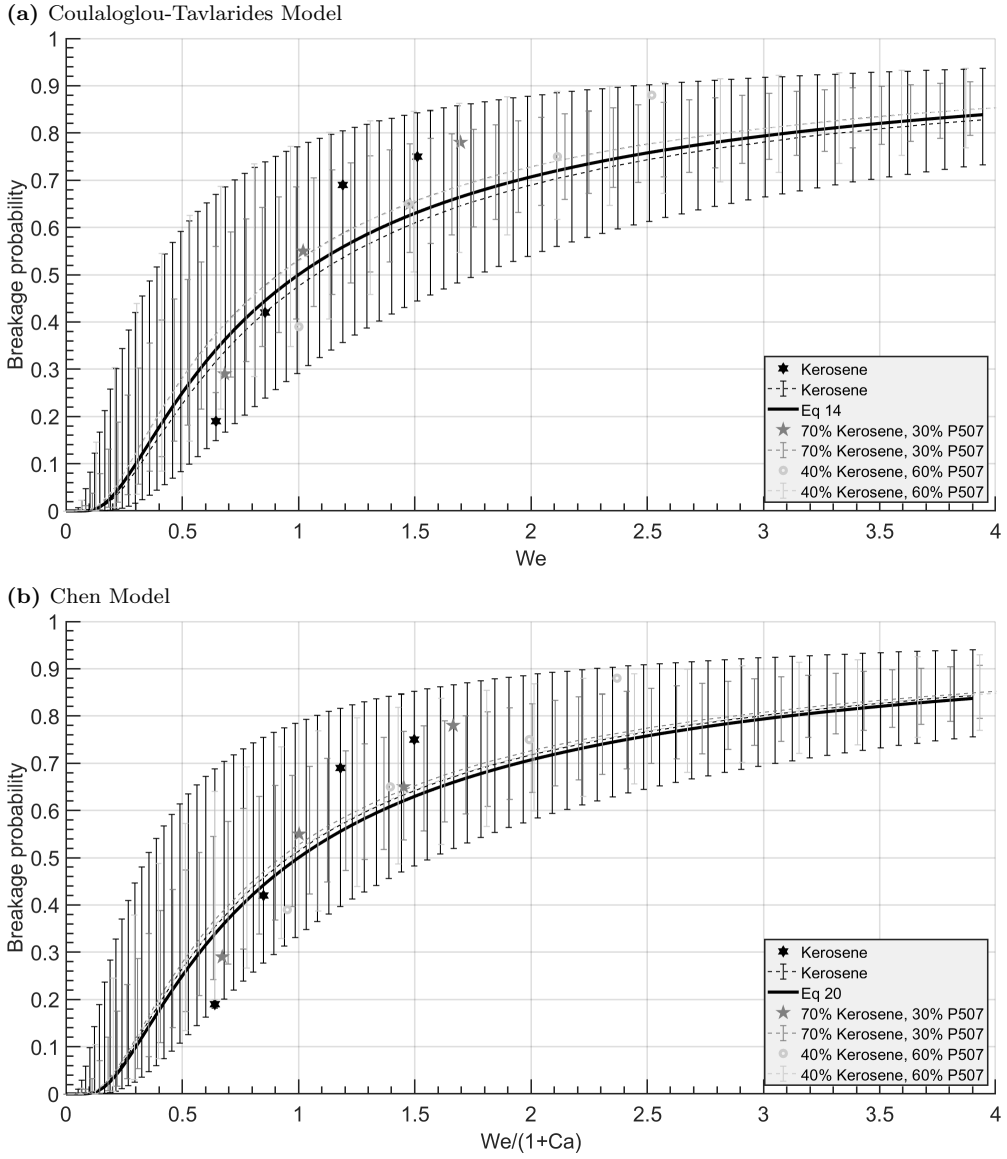

Figure 2: Breakage probability as a function of We and Ca for kerosene-water and kerosene-surfactant-water emulsions. Solid lines represent predictions using Eqs. (14) and (20), dashed lines represent regressions to experimental data, and symbols represent experimental data. Error bars represent 95% confidence intervals for the regressions.

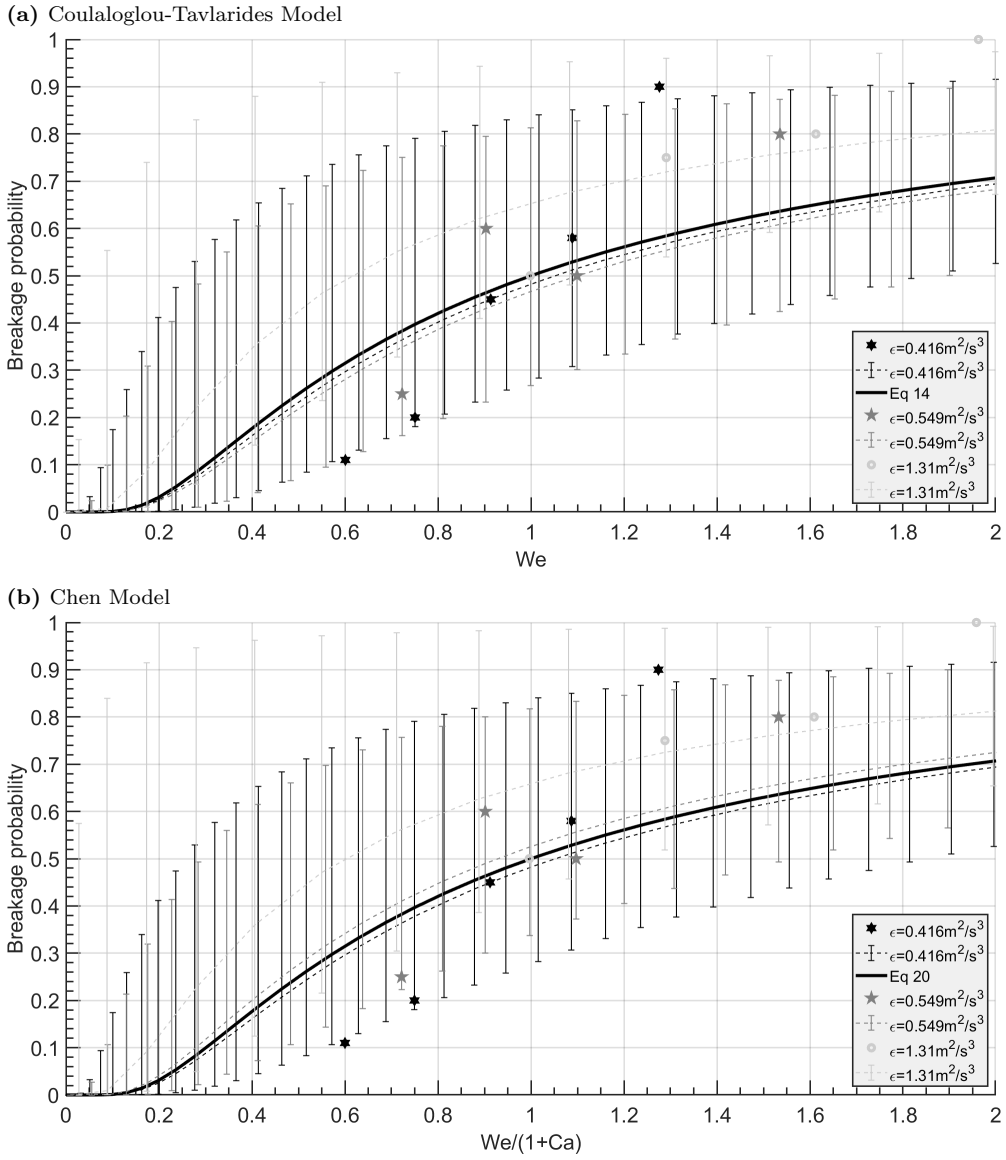

Figure 3: Breakage probability as a function of We and Ca for heptane-water emulsions. Solid lines represent predictions using Eqs.(14) and (20), dashed lines represent regressions to experimental data, and symbols represent experimental data. Error bars represent 95% confidence intervals for the regressions.

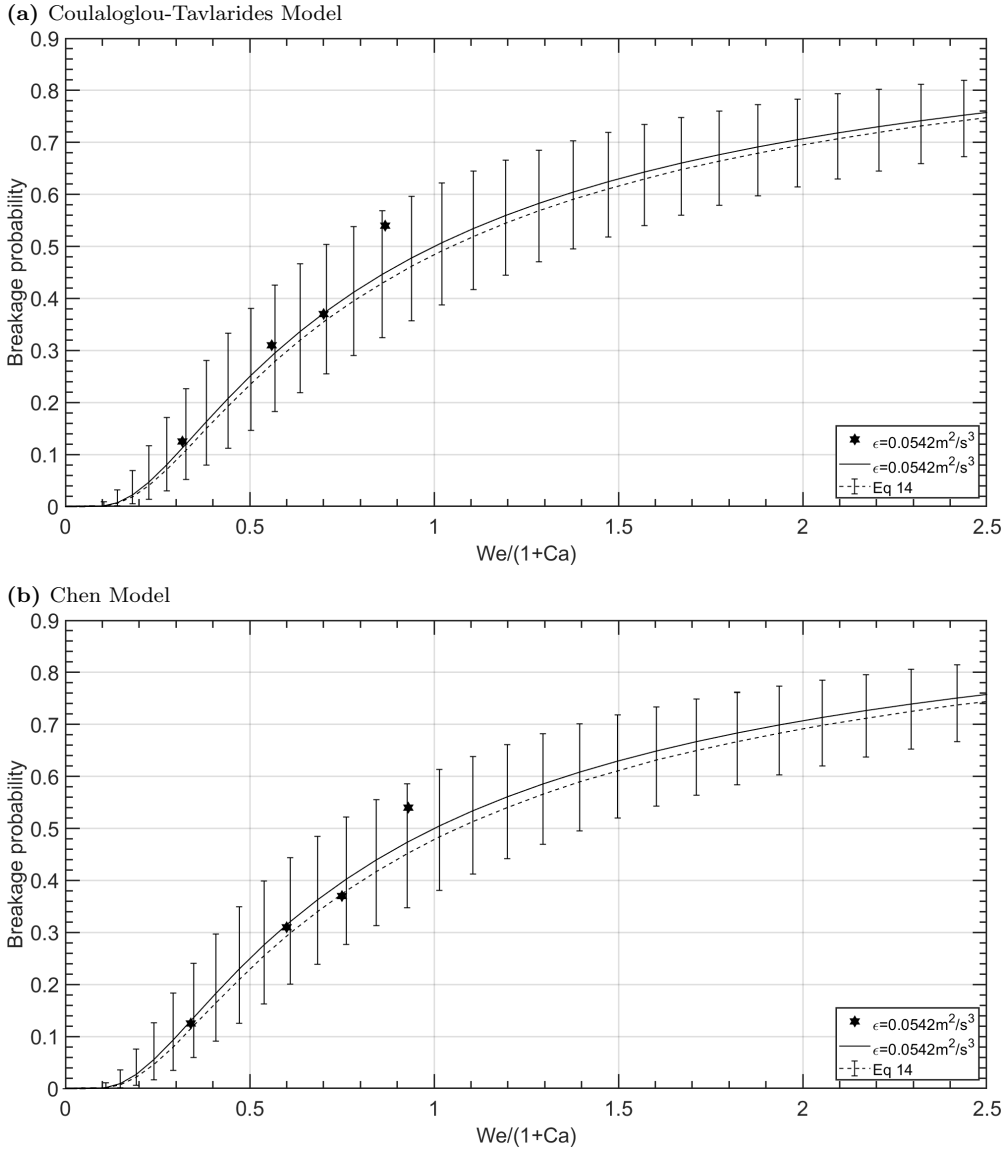

Figure 4: Breakage probability as a function of We and Ca for octanol-water emulsions. Solid lines represent predictions using Eqs.(14) and (20), dashed lines represent regressions to experimental data, and symbols represent experimental data. Error bars represent 95% confidence intervals for the regressions.

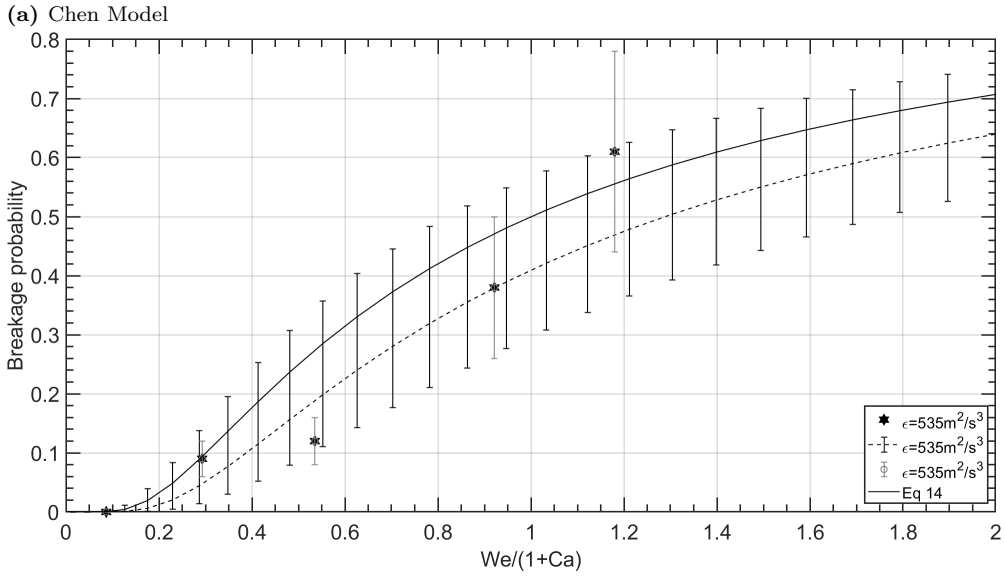

Figure 5: Breakage probability as a function of We and Ca for Rapseed oil-water emulsions. Solid lines represent predictions using Eqs.(14) and (20), dashed lines represent regressions to experimental data, and symbols represent experimental data. Error bars represent 95% confidence intervals for the regressions.

probability for the fluids considered here. The small impact of the restorative internal viscous stress compared with the interfacial stress is evident from the small values of the capillary number, Ca, listed in Table 1. In all cases considered, Ca is at least one or even two orders of magnitude smaller than the corresponding Weber numbers. In the Chen model for breakage probability, Eq. (10), the impact of drop viscosity on breakage probability depends upon the ratio Ca/We, and because this quantity is $<<$ 1 for the fluid pairs listed in Table 1, this expression converges to the Coulaloglou model for breakage probability given by Eq.(8).

Table 3: Root mean squared errors of Coulaloglou-Tavlarides and Chen model predictions using Eqs. (13) and (18) compared with experimental data for breakage probability.

Test fluid	**RMSE, (Coulaloglou-Tavlarides Model)**	**RMSE (Chen Model)**
Petroleum	0.120	0.175
Toulene	0.099	0.103
Kerosene	0.117	0.117
70% Kerosene +30% P507	0.073	0.074
40% Kerosene +60% P507	0.085	0.086
Heptane ε=0.416 m^2/s^3	0.120	0.193
Heptane ε=0.549 m^2/s^3	0.126	0.126
Heptane ε=1.31 m^2/s^3	0.185	0.186

3.2. Validation Using Experimental Data in a Homogeneous System

In a study conducted by Ravichandar *et al.* [35], a von Kármán swirling flow device was used to produce homogeneous, low intensity turbulence suitable for carrying out droplet

breakage experiments. Individual droplets of known, adjustable, and repeatable sizes were introduced one at a time into the device and high-speed optical methods and image analysis were used to capture and analyze breakage events. Several vegetable oil-water systems were investigated using canola, safflower, sesame and peanut oil as the dispersed phase, and droplet breakage probabilities were measured by analyzing thousands of droplet breakage events. This previously reported data is augmented here with new experiments carried out in the same von Kármán box in order to validate the breakage probability predictions based upon Eqs.(2), (6), (13), and (18). The new data were collected for canola oil droplets undergoing breakage at turbulence dissipation rates ε of 0.192 m^2/s^3 and 0.235 m^2/s^3, as well as for peanut oil droplets with $\varepsilon = 0.083$ m^2/s^3 and 0.192 m^2/s^3.

Physical properties and flow parameters of the vegetable oil-water fluid pairs are listed in Table 4. A comparison of the Weber and capillary numbers in Table 4 with those in

Table 4: Vegetable oil in water fluid properties and operating parameters.

Droplet Phase	ρ **(kg/m^3)**	σ **(mN/m)**	μ **(mPa·s)**	ε **(m^2/s^3)**	d **(mm)**	**We**	**Ca**
Canola Oil	915	0.018	65.9	0.083	1.88 - 3.60	0.21 - 4.2	0.236 - 0.428
				0.107	1.65 - 3.13	0.25 - 5.0	0.260 - 0.466
				0.192	1.55 - 4.34	0.37 - 7.3	0.310 - 0.570
				0.235	1.51 - 3.69	0.42 - 8.4	0.330 - 0.610
Safflower Oil	921	0.031	71.1	0.083	0.73 - 5.74	0.12 - 2.4	0.147 - 0.267
				0.107	0.62 - 5.73	0.14 - 2.9	0.160 - 0.291
Sesame Oil	946	0.011	43.3	0.083	1.39 - 3.01	0.34 - 6.8	0.249 - 0.453
				0.107	1.03 - 2.87	0.41 - 8.1	0.271 - 0.493
Peanut Oil	910	0.025	80.6	0.083	1.90 - 3.70	0.015 - 3.0	0.211 - 0.383
				0.192	1.80 - 4.00	0.031 - 6.1	0.300 - 0.543

Table 1 shows that the stabilizing internal viscous stress can be expected to play a significant role in determining breakage probability of vegetable oil droplets in water, in contrast with the petrochemical fluids considered in Section 3.1. Note that the lower and upper bounds reported for We and Ca in Table 4 correspond to the smallest and largest parent droplets considered in each experiment. Because We and Ca increase with droplet diameter according to the following proportionalities, We $\sim d^{5/3}$ and Ca $\sim d^{1/3}$, the Weber number increases more rapidly with parent diameter. As a consequence, the ratio Ca/We < 1 for the largest droplets considered, whereas generally Ca/We > 1 for the smallest parent droplets studied. Therefore, it can be anticipated that the Chen model, Eq.(10), which accounts for the stabilizing effect of the internal phase viscosity, is better suited than the Coulaloglou-Tavlarides model for predicting breakage probability for these fluid pairs, at least for small parent droplet sizes.

Fitted values for the breakage probability constants C_2 and C_3 can be obtained by regressing the Chen model, Eq. (10), to droplet breakage probability data. The resulting best-fit breakage probability plots are depicted in Figures 6 - 8, and as before, the error bars depict 95% confidence intervals. Corresponding fitted values for C_2 and C_3 are listed in Table 5, and the indicated uncertainties in this table again represent 95% confidence ranges. Breakage probability curves obtained using the analytical expressions for C_2 and C_3 given by Eqs. (13) and (18) are also shown in Figs. 6 - 8, and the values of these constants are listed in Table 5.

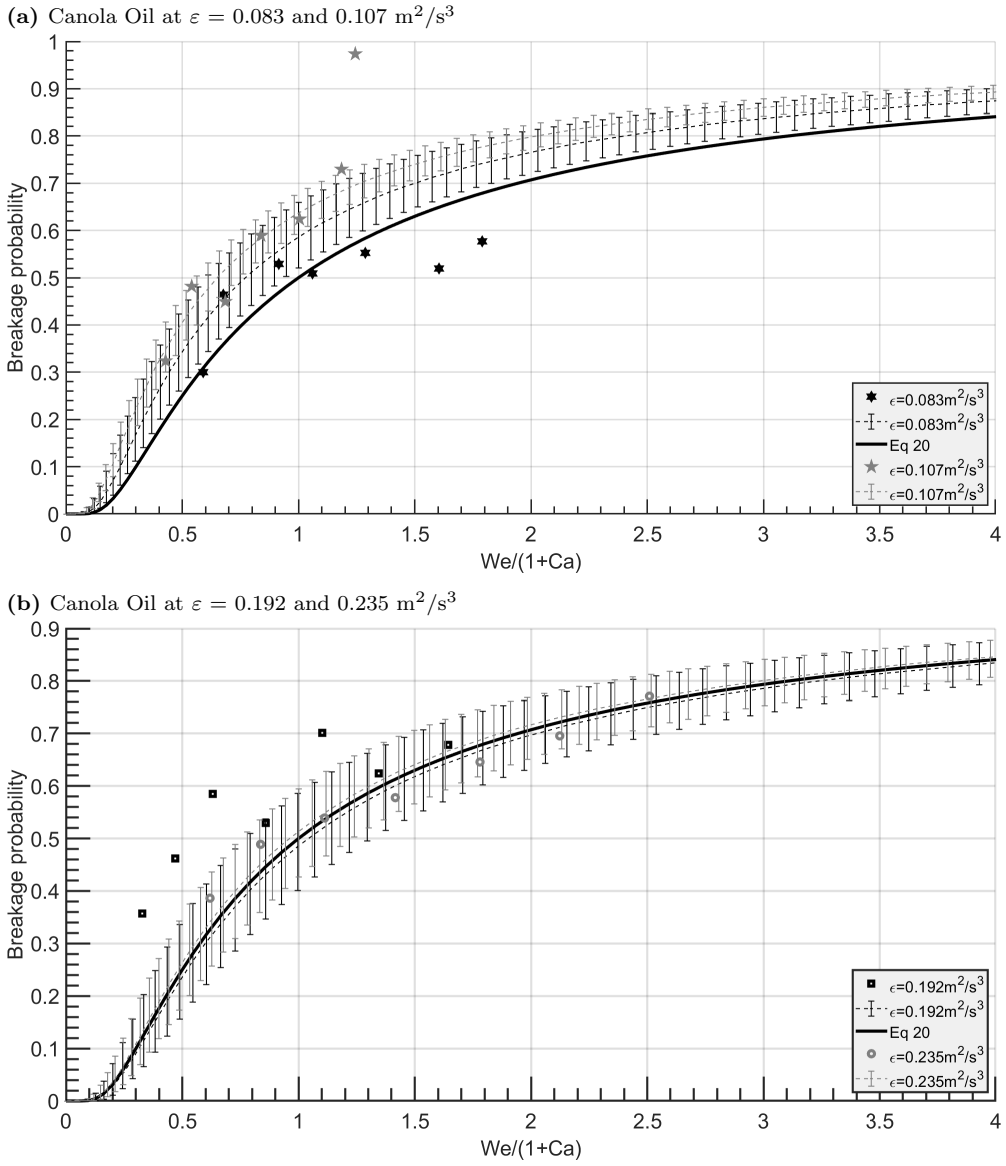

Figure 6: Breakage probability as a function of We and Ca for Canola at (a) $\varepsilon = 0.083$ and 0.107 m^2/s^3 and (b) $\varepsilon = 0.192$ and 0.235 m^2/s^3. Solid lines represents predictions using Eqs. (20); dashed lines represent regressions to experimental data. The symbols represent the experimental data and the error bars depict 95% confidence interval envelopes.

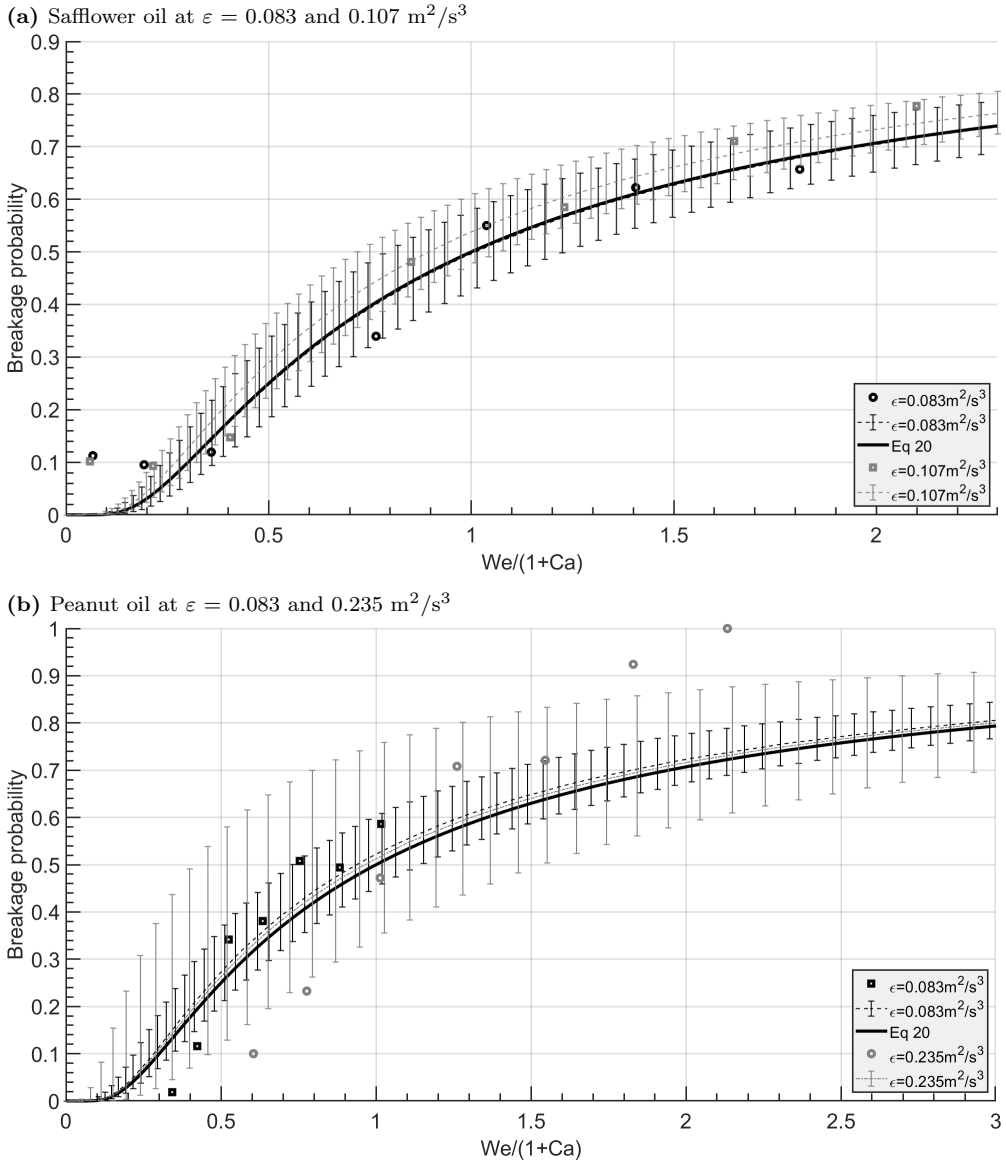

Figure 7: Breakage probability as a function of We and Ca for (a) safflower oil at $\varepsilon = 0.083$ and 0.107 m^2/s^3 and (b) peanut oil at $\varepsilon = 0.083$ and 0.235 m^2/s^3. Solid lines represent predictions using Eq. (20), and dashed lines represent regressions to experimental data. Symbols represent experimental data, and error bars depict 95% confidence interval envelopes.

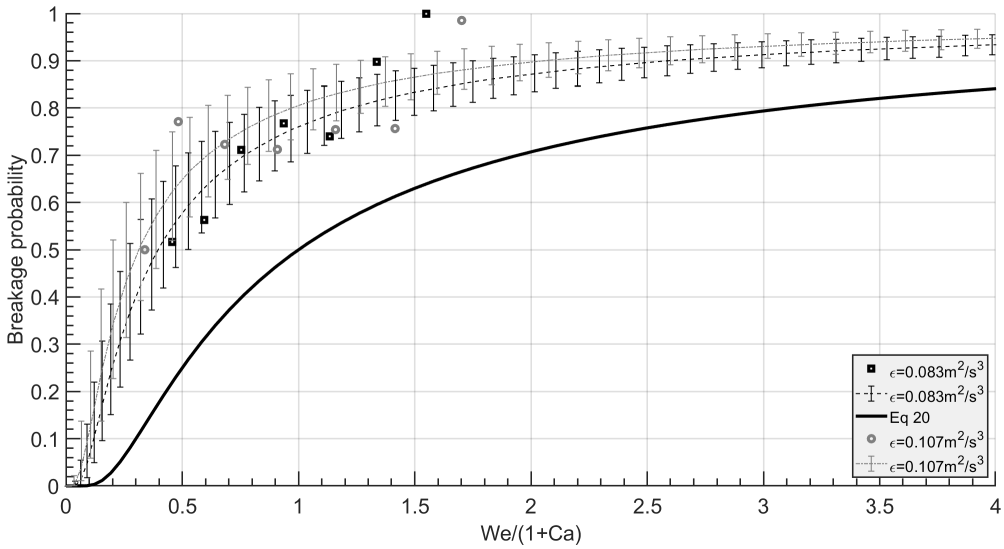

Figure 8: Breakage probability as a function of We and Ca for sesame oil at $\varepsilon = 0.083$ and 0.107 m^2/s^3. The solid line represents Eq. (20), whereas dashed lines represent regressions to experimental data. Symbols represent experimental data and error bars depict 95% confidence interval envelopes.

Table 5: Comparison of C_2 and C_3 values obtained from predictions of Eqs. (13) and (18) with values obtained by regressing the Chen model to experimental data.

Canola Oil				
ε, $\mathbf{m^2/s^3}$	C_2, **Eq.**(13)	C_2, **Regressed**	C_3 **Eq.**(18)	C_3, **Regressed**
0.083	0.3171	0.2453 ± 0.0541	0.4688	0.3627 ± 0.0799
0.107	0.3171	0.2070 ± 0.0297	0.4688	0.3606 ± 0.0438
0.192	0.3171	0.3313 ± 0.0865	0.4688	0.4898 ± 0.1279
0.235	0.3171	0.3058 ± 0.0762	0.4688	0.4521 ± 0.1126
Safflower Oil				
0.083	0.3192	0.3237 ± 0.0705	0.4704	0.4770 ± 0.1038
0.107	0.3192	0.2868 ± 0.0565	0.4704	0.4226 ± 0.0833
Peanut Oil				
0.083	0.3154	0.2964 ± 0.0656	0.4676	0.4394 ± 0.0973
0.1919	0.3154	0.3046 ± 0.01780	0.4676	0.4516 ± 0.2639
Sesame Oil				
0.083	0.3279	0.1300 ± 0.0427	0.4767	0.1890 ± 0.0621
0.107	0.3279	0.1026 ± 0.0398	0.4767	0.1492 ± 0.0579

Examination of breakage constants listed in Table 5 reveals that in most cases the values computed using Eqs. (13) and (18) are similar to those obtained by regression to experimental data, and these similarities are reflected in some of the breakage probability curves in Figs. 6 - 8. However, for sesame oil droplets the differences in the values of predicted and regressed breakage parameters are significant. Specifically, the values of C_2 and C_3 predicted by Eqs. (13) and (18) are much larger than those obtained from regression, which in turn leads to predicted breakage probability curves that rise less quickly with droplet size than do the experimental observations, as shown in Fig. 8.

A potential explanation is that the stabilizing effect of the internal viscous stress is overestimated for the sesame oil experiments, but a review of the Weber and capillary numbers listed in Table 5 does not suggest that the relative values of these dimensionless quantities are different than for the other fluids tested. However, sesame oil-water has the lowest interfacial tension among the test fluids considered here, and the accurate measurement of low values of interfacial tension can be difficult. Specifically, small errors in measurement of the droplet-water interface shape in the pendant drop method that was used here can lead to significant errors in the computed value of σ.

Although inaccurate measurement of low interfacial tension may at least partly explain discrepancies in the predicted and fitted sesame oil breakage probability curves shown in Fig. 8, another factor may be responsible. Specifically, sesame oil droplets were observed to undergo significantly larger stretching deformation before rupture when compared to the other fluids tested. Consequently, it may be the case that turbulent eddies with characteristic sizes larger than the undeformed spherical parent droplet (in violation of assumptions of both the Coulaloglou-Tavlarides and Chen models) are efficacious for causing sesame oil droplet breakage. Hence, discrepancies in the predicted and observed sesame oil droplet breakage probabilities may be due to inherent limitations and assumptions of the Chen model.

4. Conclusions

Analytical expressions for evaluating parameters in two well-known models for liquid-liquid droplet breakage probability were developed by employing dimensional analysis and by hypothesizing a condition for droplets to have equal probability of undergoing breakage or remaining stable. The validity of these expressions was evaluated by comparing droplet breakage predictions for a variety of fluid pairs with experimental data published previously and with new droplet breakage data obtained using a von Kármán box. The droplet breakage probabilities found from experiments were generally well-predicted by the Coulaloglou-Tavlarides and Chen models when using Eqs. (13) and (18) for the breakage constants, C_2 and C_3. However breakage probabilities were underpredicted for sesame oil, and to a lesser extent for canola oil, at low turbulence dissipation rates. The observation that significant droplet stretching occurs in these cases is consistent with the hypothesis that turbulent eddies larger than the parent droplet play a significant role in causing droplet breakage, thereby contradicting an important assumption underlying the Coulaloglou-Tavlarides and Chen models. Inclusion of these larger eddies in droplet breakage analysis would be expected

to produce predictions of elevated breakage probabilities when compared to these standard models.

5. Acknowledgments

The authors wish to acknowledge helpful discussions with Prof. Rodney O. Fox and Dr. Manjil Ray, as well as assistance in carrying out some experiments by Annika Lehan. The authors also acknowledge support for this work by BASF and by award 2201707 from the National Science Foundation.

References

[1] D. Maggioris, A. Goulas, A. Alexopoulos, E. Chatzi, C. Kiparissides, Prediction of particle size distribution in suspension polymerization reactors: effect of turbulence nonhomogeneity, Chemical Engineering Science 55 (20) (2000) 4611–4627. doi:https://doi.org/10.1016/S0009-2509(00)00100-7.
URL https://www.sciencedirect.com/science/article/pii/S0009250900001007

[2] D. J. McClements, Food Emulsions, CRC Press, 2015. doi:10.1201/b18868.
URL https://doi.org/10.1201/b18868

[3] E. H. Herø, N. L. Forgia, J. Solsvik, H. A. Jakobsen, Single drop breakage in turbulent flow: Statistical data analysis, Chemical Engineering Science: X 8 (11 2020). doi:10.1016/j.cesx.2020.100082.

[4] S. Nachtigall, D. Zedel, M. Kraume, Analysis of drop deformation dynamics in turbulent flow, Chinese Journal of Chemical Engineering 24 (2016) 264–277. doi:10.1016/j.cjche.2015.06.003.

[5] I. D. Nissanka, P. D. Yapa, Calculation of oil droplet size distribution in ocean oil spills: A review, Marine Pollution Bulletin 135 (2018) 723–734. doi:https://doi.org/10.1016/j.marpolbul.2018.07.048.
URL https://www.sciencedirect.com/science/article/pii/S0025326X18305356

[6] C. Li, J. Miller, J. Wang, S. S. Koley, J. Katz, Size distribution and dispersion of droplets generated by impingement of breaking waves on oil slicks, Journal of Geophysical Research: Oceans 122 (10) (2017) 7938–7957. arXiv:https://agupubs.onlinelibrary.wiley.com/doi/pdf/10.1002/2017JC013193, doi:https://doi.org/10.1002/2017JC013193.
URL https://agupubs.onlinelibrary.wiley.com/doi/abs/10.1002/2017JC013193

[7] P. A. Quadros, C. M. Baptista, Effective interfacial area in agitated liquid–liquid continuous reactors, Chemical Engineering Science 58 (17) (2003) 3935–3945. doi:https://doi.org/10.1016/S0009-2509(03)00302-6.
URL https://www.sciencedirect.com/science/article/pii/S0009250903003026

[8] Y. Liao, D. Lucas, A literature review of theoretical models for drop and bubble breakup in turbulent dispersions, Chemical Engineering Science 64 (15) (2009) 3389–3406. doi:https://doi.org/10.1016/j.ces.2009.04.026.
URL https://www.sciencedirect.com/science/article/pii/S0009250909002759

[9] M. Karimi, R. Andersson, An exploratory study on fluid particles breakup rate models for the entire spectrum of turbulent energy, Chemical Engineering Science 192 (2018) 850–863. doi:https://doi.org/10.1016/j.ces.2018.08.016.
URL https://www.sciencedirect.com/science/article/pii/S0009250918305852

[10] M. Karimi, R. Andersson, Dual mechanism model for fluid particle breakup in the entire turbulent spectrum, AIChE Journal 65 (8) (2019) e16600. doi:https://doi.org/10.1002/aic.16600.
URL https://aiche.onlinelibrary.wiley.com/doi/abs/10.1002/aic.16600

[11] S. Castellano, L. Carrillo, N. Sheibat-Othman, D. Marchisio, A. Buffo, S. Charton, Using the full turbulence spectrum for describing droplet coalescence and breakage in industrial liquid-liquid systems: Experiments and modeling, Chemical Engineering Journal 374 (2019) 1420–1432. doi:https://doi.org/10.1016/j.cej.2019.06.032.
URL https://www.sciencedirect.com/science/article/pii/S1385894719312902

[12] H. Zhang, G. Yang, A. Sayyar, T. Wang, An improved bubble breakup model in turbulent flow, Chemical Engineering Journal 386 (4 2020). doi:10.1016/j.cej.2019.04.064.

[13] H. K. Foroushan, H. A. Jakobsen, Experimental study of single bubble breakage in turbulent flow field: Evaluation of breakage models, Chemical Engineering Science 253 (2022) 117584. doi:https://doi.org/10.1016/j.ces.2022.117584.
URL https://www.sciencedirect.com/science/article/pii/S0009250922001683

[14] E. H. Herø, N. La Forgia, J. Solsvik, H. A. Jakobsen, Single drop breakage in turbulent flow: Statistical data analysis, Chemical Engineering Science: X 8 (2020) 100082. doi:https://doi.org/10.1016/j.cesx.2020.100082.
URL https://www.sciencedirect.com/science/article/pii/S2590140020300289

[15] S. Galinat, O. Masbernat, P. Guiraud, C. Dalmazzone, C. Noïk, Drop break-up in turbulent pipe flow downstream of a restriction, Chemical Engineering Science 60 (2005). doi:10.1016/j.ces.2005.05.012.

[16] S. Galinat, L. G. Torres, O. Masbernat, P. Guiraud, F. Risso, C. Dalmazzone, C. Noik, Breakup of a drop in a liquid-liquid pipe flow through an orifice, AIChE Journal 53 (2007). doi:10.1002/aic.11055.

[17] S. Maaß, M. Kraume, Determination of breakage rates using single drop experiments, Chemical Engineering Science 70 (2012) 146–164. doi:10.1016/j.ces.2011.08.027.

[18] R. Andersson, B. Andersson, Modeling the breakup of fluid particles in turbulent flows, AIChE Journal 52 (2006). doi:10.1002/aic.10832.

[19] J. Solsvik, S. Tangen, H. A. Jakobsen, On the constitutive equations for fluid particle breakage, Reviews in Chemical Engineering 29 (5) (2013) 241–356 [cited 2022-10-21]. doi:doi:10.1515/revce-2013-0009.
URL https://doi.org/10.1515/revce-2013-0009

[20] M. Ashar, D. Arlov, F. Carlsson, F. Innings, R. Andersson, Single droplet breakup in a rotor-stator mixer, Chemical Engineering Science 181 (2018) 186–198. doi:https://doi.org/10.1016/j.ces.2018.02.021.
URL https://www.sciencedirect.com/science/article/pii/S0009250918300836

[21] B. O. Hasan, Single bubble breakage in oil under stirring conditions, Al-Nahrain Journal for Engineering Sciences 25 (1) (2022) 6–11.

[22] A. M. Mhawesh, B. O. Hasan, H. Znad, Hydrodynamics of stirred tank and bubble breakup behavior induced by rushton turbine, Al-Nahrain Journal for Engineering Sciences 25 (1) (2022) 35–43.

[23] H. A. Alabdly, H. S. Majdi, M. F. Hamad, M. M. Hathal, B. O. Hasan, Effect of impeller geometry on bubble breakage and the contributions of different breakage mechanisms in a stirred tank, Fluid Dynamics Research 52 (6) (2020) 065504.

[24] A. Sathyagal, D. Ramkrishna, G. Narsimhan, Droplet breakage in stirred dispersions. breakage functions from experimental drop-size distributions, Chemical Engineering Science 51 (9) (1996) 1377–1391, festschrift for Professor R. Byron Bird. doi:https://doi.org/10.1016/0009-2509(95)00311-8.
URL https://www.sciencedirect.com/science/article/pii/0009250995003118

[25] C. Y. Wang, R. V. Calabrese, Drop breakup in turbulent stirred-tank contactors. part ii: Relative influence of viscosity and interfacial tension, AIChE Journal 32 (4) (1986) 667–676. arXiv:https://aiche.onlinelibrary.wiley.com/doi/pdf/10.1002/aic.690320417, doi:https://doi.org/10.1002/aic.690320417.
URL https://aiche.onlinelibrary.wiley.com/doi/abs/10.1002/aic.690320417

[26] T. Lemenand, D. D. Valle, P. Dupont, H. Peerhossaini, Turbulent spectrum model for drop-breakup mechanisms in an inhomogeneous turbulent flow, Chemical Engineering Science 158 (2017). doi:10.1016/j.ces.2016.09.031.

[27] C. Coulaloglou, L. Tavlarides, Description of interaction processes in agitated liquid-liquid dispersions, Chemical Engineering Science 32 (1977) 1289–1297. doi:10.1016/0009-2509(77)85023-9.

[28] A. Kolmogorov, Die lokale struktur der turbulenz in einer inkompressiblen zähen flüssigkeit bei sehr großen reynoldsschen zahlen, Compt. Rend. Acad. Sc. USSR 30 (4) (1958).

[29] A. Kolmogorov, Die energiedissipation für lokalisotrope turbulenz, in: Dokl. Akad. Nauk SSSR, Vol. 32, 1958, pp. 16–18.

[30] Z. Chen, J. Prüss, H. J. Warnecke, A population balance model for disperse systems: Drop size distri-

bution in emulsion, Chemical Engineering Science 53 (1998). doi:10.1016/S0009-2509(97)00328-X.

[31] J. O. Hinze, Fundamentals of the hydrodynamic mechanism of splitting in dispersion processes, AIChE Journal 1 (1955). doi:10.1002/aic.690010303.

[32] N. Lebaz, F. Azizi, N. Sheibat-Othman, Modeling droplet breakage in continuous emulsification using static mixers in the framework of the entire spectrum of turbulent energy, Industrial & Engineering Chemistry Research 61 (1) (2022) 541–553. doi:10.1021/acs.iecr.1c03529.

[33] J. Zhang, Y. Wang, G. W. Stevens, W. Fei, A state-of-the-art review on single drop study in liquid–liquid extraction: Experiments and simulations, Chinese Journal of Chemical Engineering 27 (2019) 2857–2875. doi:10.1016/j.cjche.2019.03.025.

[34] Y. Ji, J. Bellettre, A. Montillet, P. Massoli, Experimental investigation on single drop breakage in two-stream impinging microchannels, Experiments in Fluids 62 (1) (2021) 1–23.

[35] K. Ravichandar, R. D. Vigil, R. O. Fox, S. Nachtigall, A. Daiss, M. Vonka, M. G. Olsen, Turbulent droplet breakage in a von kármán flow cell, Physics of Fluids 34 (7) (2022) 073319. arXiv:https://doi.org/10.1063/5.0096395, doi:10.1063/5.0096395.
URL https://doi.org/10.1063/5.0096395